Fuel 392 (2025) 134827

Contents lists available at ScienceDirect

Fuel

journal homepage: www.elsevier.com/locate/jfue

Full length article

Experimental determination of quantitative yields from polymethyl methacrylate (PMMA) flash pyrolysis in a fluidized bed reactor via online FTIR gas analysis

Stefan Pielsticker[a,*], Katja Hendricks[a], Christoph Knevels[a], Marcus S. Lehnertz[b], Regina Palkovits[b,c,d], Reinhold Kneer[a]

[a] Institute of Heat and Mass Transfer (WSA), RWTH Aachen University, Augustinerbach 6, 52056 Aachen, Germany
[b] Institute of Technical and Macromolecular Chemistry (ITMC), RWTH Aachen University, Worringerweg 2, 52074 Aachen, Germany
[c] Institute for a Sustainable Hydrogen Economy (INW-2), Forschungszentrum Jülich, Marie-Curie-Str. 5, 52428 Jülich, Germany
[d] Max-Planck-Institute for Chemical Energy Conversion, Stiftstr. 34–36, 45470 Mülheim an der Ruhr, Germany

HIGHLIGHTS

- New FTIR calibration enables precise quantitative detection of MMA in the gas phase.
- Very good closure of mass and elemental balance is achieved for PMMA pyrolysis.
- MMA yield drops from 0.9 to 0.5 by increasing the temperature from 673 to 873 K.
- MMA yield is controlled by primary pyrolysis and secondary gas-phase reactions.
- High MMA purity in the condensate highlights potential for closed-loop recycling.

ARTICLE INFO

Keywords:
PMMA pyrolysis
Fluidized bed reactor
Online FTIR gas analysis
Monomer recovery
Primary and secondary demposition

ABSTRACT

Chemical recycling processes, such as pyrolysis, have the potential to break down the polymer (e.g., polymethyl methacrylate, PMMA) into its main building blocks (monomers), and thus enable the preservation of full functionality in closed-loop recycling processes. In this study, products from flash pyrolysis of PMMA are quantitatively determined using an ex situ exhaust gas analysis by means of Fourier-transform infrared (FTIR) spectroscopy. To achieve this, the FTIR is additionally calibrated for methyl methacrylate (MMA) with an MMA/N_2 mixture of various concentrations. Flash pyrolysis conditions (heating rates approximately 10^3 K s^{-1}) are realized with a small-scale fluidized bed reactor operated with a nitrogen atmosphere and temperatures between 573 and 873 K with a continuous feed of PMMA granules. The experiments reveal MMA yields up to 90 % at 673 K. With increasing temperature, the MMA yield drops to approximately 50 % at 873 K. In return, the yields of the MMA decomposition products such as carbon dioxide (CO_2), methane (CH_4), carbon monoxide (CO), propylene (C_3H_6), and formaldehyde (CH_2O) increase. The approximated residence time of 20–30 s leads to a stronger decomposition of the MMA into its fragments (especially at higher temperatures) than in other studies, which can be well modeled with a single first-order decomposition mechanism. A detailed analysis of captured condensate reveals a high purity of MMA, which enables the feedback into the polymerization process.

1. Introduction

Plastics have become an integral part of our daily lives, but their usage also raises several global issues. These include the depletion of fossil resources, the emission of CO_2 during production, and environmental pollution resulting from improper disposal. Consequently, there is a pressing need for efficient and environmentally friendly recycling strategies for plastic waste [1,2]. Most of the currently available techniques focus either on purely energetic use within combustion or mechanical recycling, where the waste is sorted, cleaned, and then fed back

* Corresponding author.
Email address: pielsticker@wsa.rwth-aachen.de (S. Pielsticker).

https://doi.org/10.1016/j.fuel.2025.134827
Received 18 September 2024; Received in revised form 15 November 2024; Accepted 19 February 2025
Available online 10 March 2025

into the production process as shredded material [2,3]. This process is limited to certain types of plastics, may be sensitive to impurities and mixed plastics, and leads to a degradation of material quality in each cycle [4]. To preserve the full functionality of the polymer, chemical recycling is required, where the plastic waste is broken down into its main building blocks and then repolymerized [4]. One viable option to treat plastic waste is pyrolysis, a thermal process that occurs in the absence of oxygen, which enables valorizing the feedstock again by breaking it into monomers and other chemically useful products [5,6]. These products may also enable the option to leave the plastic circle by adding additional mass flows (e.g., biomass or H_2) and renewable energy to produce new, more valuable chemical products. The present study should build the basis to evaluate the potential of polymethyl methacrylate (PMMA) pyrolysis to contribute to chemical recycling or up-cycling. PMMA is a transparent and rigid thermoplastic polymer often used as a lightweight alternative to glass [7]. In 2020, the annual world production of PMMA was around 2.4×10^6 t, while only 3.0×10^4 t (1.25 %) have been recycled [4]. For Europe, the recycling rate is slightly higher and reaches approximately 2.6 % [8] but still requires major development efforts to achieve a circular economy. In a life cycle analysis, Kikuchi et al. [9] highlight that monomer recovery has the highest potential for closed-loop recycling of PMMA.

During PMMA pyrolysis, the polymer is decomposed into different reaction products, whereby the product spectrum and the observed yields strongly depend on the reaction temperature. At moderate temperatures below 750 K, the main reaction product is the monomer methyl methacrylate (MMA). Different studies have reported MMA yields up to approximately 97 % [10–12]. With increasing temperature, the decomposition of the monomer proceeds into different fragments, whereby the main products are CO, CO_2, CH_4, and C_3H_6 [10–12]. Besides these main products, a wide range of other decomposition products in the liquid phase (e.g., methacrylate, methyl isobutyrate, methacrylic acid, methyl propionate, or methanol [10,11,13]) and in the gaseous phase (e.g., H_2, C_2H_4, C_2H_6, C_3H_8, or CH_2O [10,14]) are present. Quantitative yields are typically determined by capturing the reaction products integrally from a stationary pyrolysis process and by performing a post-pyrolysis analysis via gas chromatography coupled with mass spectroscopy [11,15].

To determine not only the integral yields but also the reaction rates, time-resolved measurements are required. One of the most common techniques is a thermogravimetric analysis (TGA), where the sample is slowly heated and weight loss is simultaneously measured [11,16,17]. These analytics mainly focus on the detailed description of the decomposing mechanism of the solid, e.g., different types of scission reactions [16]. Due to the direct measurement of the mass, an almost perfect closure of the mass balance is given for the remaining PMMA and the released total volatiles. However, TGA is limited to low heating rates and may not reflect the flash pyrolysis conditions in typical industrial- or pilot-scale apparatuses (e.g., fluidized bed reactors [10,11], extruders, or molten metal bath reactors [4]) for plastic recycling.

Online analysis of batch-wise experiments under flash pyrolysis conditions is carried out for only a very limited number of species (CO and CO_2) by Chub et al. [13]. Recently, Sanders et al. [14] determined selected pyrolysis reaction products (CH_2O, CO, and CO_2) of MMA pyrolysis in situ and highly time-resolved by means of laser absorption spectroscopy in a shock wave reactor. However, online quantitative experimental data on pyrolysis products from flash pyrolysis experiments are scarce.

Thus, the present study focuses on the quantitative determination of PMMA pyrolysis products – with the widest product spectrum possible – under flash pyrolysis conditions representing high heating rates and high temperatures. To approximate the flash pyrolysis conditions, a small-scale fluidized bed reactor (FBR) is used, which has already been proven to be well-suited for investigations of biomass flash pyrolysis [18,19]. Relevant reaction products – including all previously mentioned light gases – are measured ex situ with an online Fourier-transform infrared (FTIR) spectrometer. However, the FTIR has not been quantitatively calibrated for the expected main product MMA. Thus, a calibration method based on a systematic condensation of an MMA-loaded gas stream to its saturation point is introduced to measure reference spectra for a wide range of concentrations. The newly obtained reference spectra are then included in an upgraded evaluation procedure to quantitatively determine the pyrolysis products of PMMA. The new method is cross-checked with a non-reactive pure MMA sample and pyrolysis experiments under stationary conditions. As the analysis is based on gas-phase analytics, it allows deeper insights into the roles of primary and secondary decomposition reactions.

2. Material and methods

To quantitatively determine pyrolysis products of PMMA based on gas-phase analytics, the measurement equipment must be made capable of correctly measuring the expected reaction products. From qualitative analysis, the monomer MMA has been identified to be present in large fractions in the product spectrum. Thus, the Fourier-transform infrared spectrometer is first used to measure reference spectra of MMA vapor mixed with N_2 in different concentrations. Afterward, the calibration is cross-checked with evaporated pure MMA samples before the FTIR is coupled to a small-scale fluidized bed reactor setup for the pyrolysis experiments performed with PMMA.

2.1. Quantitative MMA calibration

To generate mixtures of MMA vapor in nitrogen, the setup shown in Fig. 1 is used. The same setup has already been successfully used to load gas streams with water vapor [20].

A nitrogen stream with a flow rate of 25 l h^{-1} (standard conditions) is first enriched with MMA vapor by bubbling through a tempered bath of liquid MMA. Afterward, the loaded nitrogen stream leaves the flask to the top through an intensive cooler whose temperature is 2–3 K lower than the MMA temperature. In this way, a saturated nitrogen stream leaves the intensive cooler because the excess MMA condensates in the intensive cooler and flows back into the round flask. By measuring the condenser outlet gas temperature, the saturation temperature T_s is measured and the saturation pressure p_s is calculated by using the Antoine equation with coefficients (for pressures inserted in bar) provided from the NIST database [21] and originally determined based on experimental data from Brockhaus and Jenckel [22]:

$$\log_{10}(p_s) = 5.37785 - \frac{1945.56\ \mathrm{K}}{T_s - 7.569\ \mathrm{K}} \tag{1}$$

The volume fraction φ_{MMA} is derived from Eq. (2) assuming ideal gas law:

$$\varphi_{MMA} = \frac{p_s(T)}{p}. \tag{2}$$

Within Eq. (2), the total pressure p = 1.026 bar reflects the ambient conditions.

Fig. 2 shows the relationship between saturation temperature and resulting MMA volume fraction. In order to achieve volume fractions above φ_{MMA} = 36,000 ppm the tempered bath is heated, while for lower target volume fractions, the bath is cooled. The shown calibration points indicate a possible range from φ_{MMA} = 5180 to 145,087 ppm. One lower concentration of φ_{MMA} = 3626 ppm could be reached by diluting the flow after the condensation in a ratio of 1:1 with N_2. However, for lower temperatures or higher dilutions, no reliable reference spectra could be recorded. One reason could be that the parameters of the Antoine equation have been derived at a higher temperature range.

Downstream of the cooler, the gas stream is immediately heated to 453 K in order to prevent further condensation of the MMA before reaching the gas cell of the FTIR spectrometer (*Ansyco GASMET DX-2000*, 2.0 m optical path length). The cell is heated to 453 K and operated under atmospheric pressure. The FTIR spectrometer records spectra in the

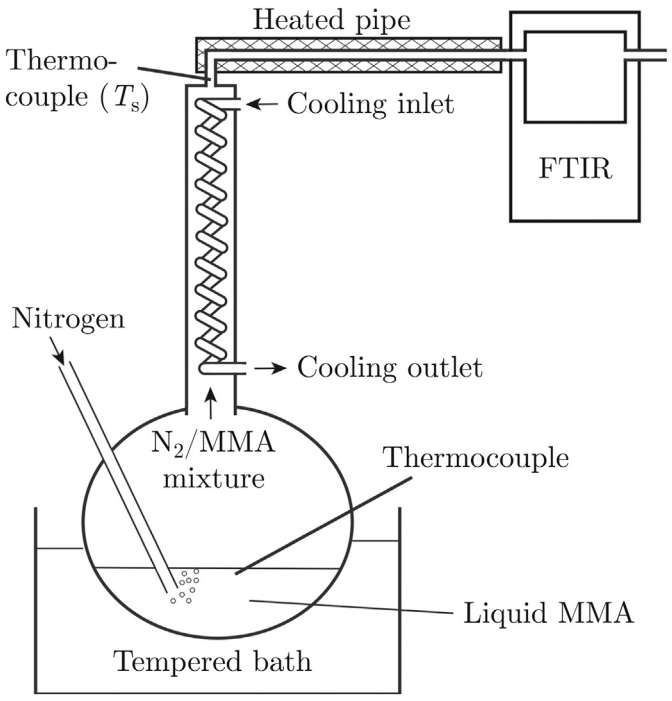

Fig. 1. Setup for quantitative MMA dosing in an N_2 stream.

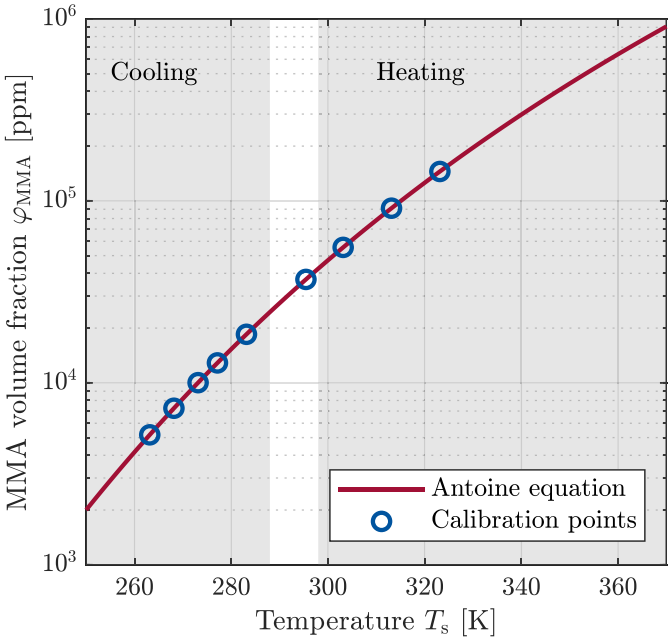

Fig. 2. Correlation between saturation temperature and MMA volume fraction.

mid-infrared wavenumber region ν = 600–4200 cm^{-1} with a spectral resolution of 8 cm^{-1}. For each calibration point, the reference spectrum is calculated as an average from 30 single spectra with a measurement time of 20 s each. Fig. 3 shows the obtained reference spectra for five selected MMA volume fractions.

Most dominant are the absorption bands of C–O–C stretching vibration (1140–1240 cm^{-1}), C=O stretching in the ester group (1735 cm^{-1}), and C–H stretching of the methyl groups (3000 cm^{-1}) similar as in the observations of Abd Karim [24]. For quantitative evaluation, wavenumber regions between 3400 and 3500 cm^{-1} as well as from 2700 and 3200 cm^{-1} have been chosen depending on the expected concentration as the absorbance gradient is here most sensitive to the concentration, and cross-correlations with other species are minimized. Regions with absorbances above $A = 1$ have been excluded due to low signal-to-noise ratio.

2.2. Validation with pure MMA

To verify the combination of newly recorded reference spectra (from Section 2.1) and range of selected wavenumbers (see Fig. 3) in the regression analysis, pure liquid MMA with a sample volume of 0.05 ml is directly injected into a heated pipe (453 K) with a flow rate of 200 l h^{-1} (standard conditions). After evaporation, the flow first passes a diffusion chamber (volume V = 6.4 l) and then the FTIR gas cell, where the IR spectra are recorded. By regression analysis between the measured spectrum and available reference spectra of known concentration, the corresponding MMA volume fraction $\varphi_{MMA}(t)$ is determined. From time-dependent measurements of an effective frequency of 0.5 Hz, the profile shown in Fig. 4 is obtained.

By using Eq. (3), the yield y_{MMA} of detected MMA is determined:

$$y_{MMA} = \frac{\rho_{N_2} \cdot M_{MMA}}{M_{N_2}} \cdot \frac{\dot{V}_{N_2}}{m_{MMA}} \cdot \int_{t=0}^{\infty} \frac{\varphi_{MMA}(t)}{1-\varphi_{MMA}(t)}\, dt \tag{3}$$

The equation includes time-constant properties such as the density of nitrogen ρ_{N_2}, the molecular mass M of MMA and N_2, the nitrogen volume flow $\dot{V}_{N_2}$, and the injected MMA mass m_{MMA} as well as the time-dependent measured MMA volume fraction $\varphi_{MMA}(t)$. Fig. 5 shows the yields for 10 repetitions of single samples using the available reference spectrum from the NIST database in comparison with the newly recorded IR spectra for evaluation. Within the repetitions, the detected MMA yield fluctuates around the mean value of 1.38 with a standard deviation of 0.08 by using the NIST database and 1.08 ± 0.06 while using the new reference spectra, leading to a 78 % better determination. The systematic slight overprediction may arise from an overestimation in the low-concentration region, where reference spectra are not available due to constraints (minimum reachable saturation temperature) of the calibration procedure.

2.3. Pyrolysis experimental setup

The experimental setup for the pyrolysis experiments consists of a laboratory-scale fluidized bed reactor connected to gas and fuel feed systems in combination with an online gas analysis system and a condensation unit in the off-stream as illustrated in Fig. 6.

The fluidized bed reactor consists of two coaxially positioned ceramic pipes pressed into a stainless-steel reactor head at the upper end. While the outer pipe is closed at the bottom end, the inner one ends with a porous sintered quartz glass distributor with a pore size of 40–100 μm. The inner pipe with a diameter of d_{FB} = 55 mm and a total length of L = 750 mm is partly filled with small aluminum oxide particles (Al_2O_3, particle diameter 100–180 μm, bed volume approx. 70 ml). According to the correlation from Abrahamsen and and Geldart [25], those particles have minimum fluidization velocities ranging from v_{min} = 0.013 to 0.016 m s^{-1} in the investigated temperature range.

During operation, these particles are fluidized by an N_2 gas stream flowing from the reactor head downwards through the annular gap between the inner and outer pipe before entering the inner pipe through the distributor. By passing through the annular gap, the gas stream (80 l h^{-1}, standard conditions) heats up to the temperature of the electrically heated furnace, where the reactor is placed in. The actual temperature in the bed is cross-checked with an S-type thermocouple. This results in a superficial velocity of v = 0.02–0.03 m s^{-1}

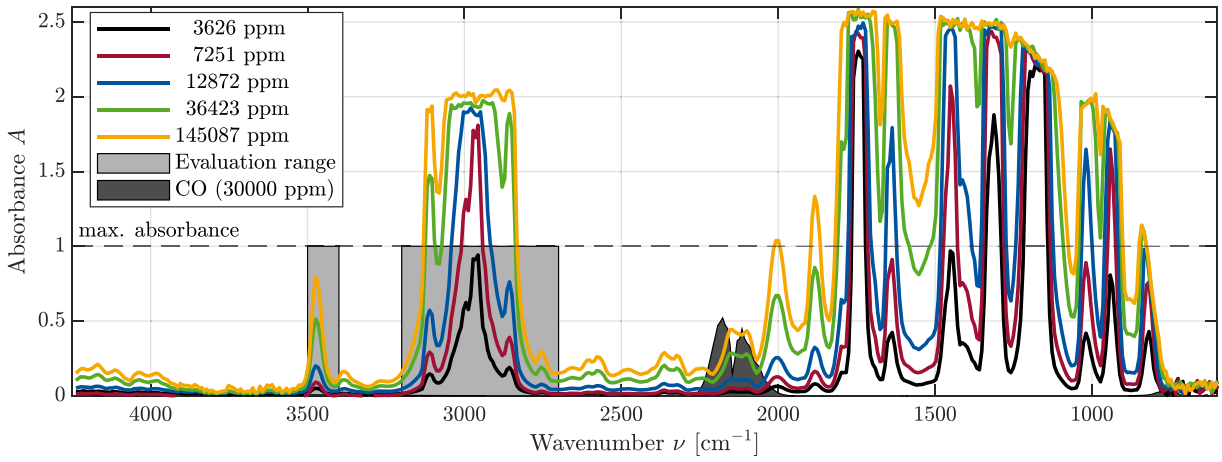

Fig. 3. Selected reference spectra of methyl methacrylate diluted in N_2 with different volume fractions ranging from 3626 to 145,087 ppm. Reference spectra are available in an open-access data publication [23]. Gray areas mark the evaluation range for quantitative MMA analysis as well as the absorption area of CO, showing strong interference with the MMA spectra. (For interpretation of the references to colour in this figure legend, the reader is referred to the web version of this article.)

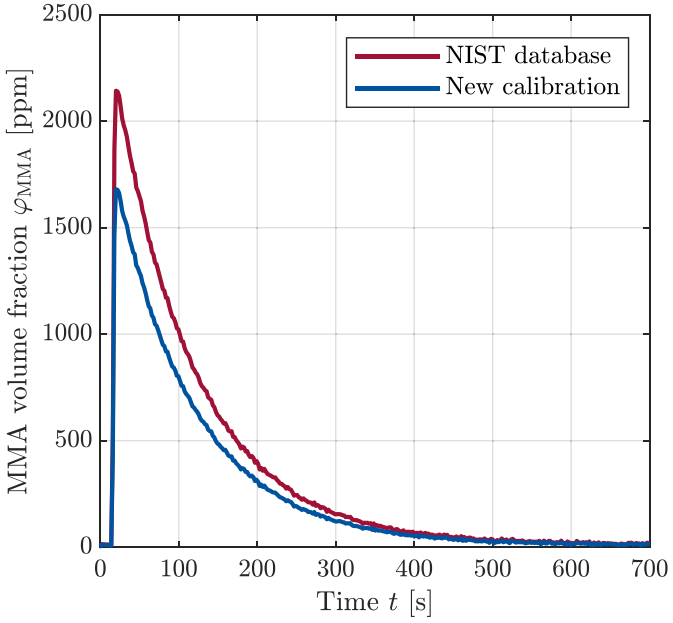

Fig. 4. Validation experiments comparing the measured MMA volume fraction from an evaporated pure MMA droplet using reference spectra from the NIST database [21] and own reference spectra [23].

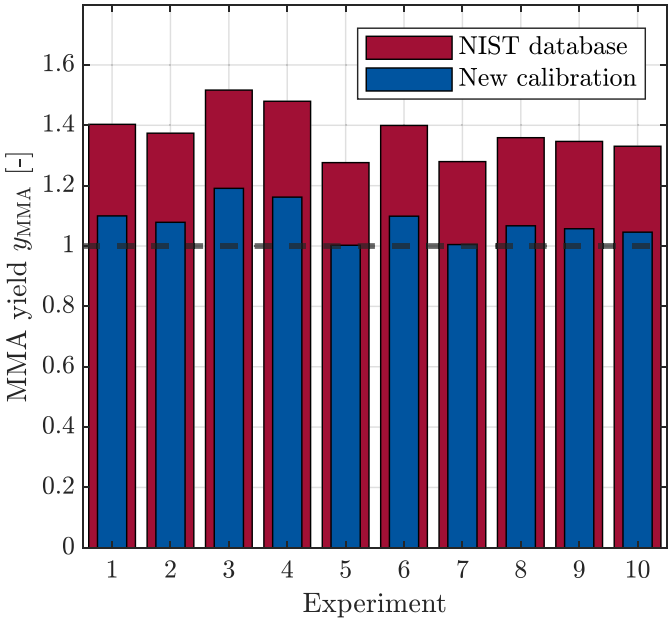

Fig. 5. Validation experiments comparing the measured MMA yield from an evaporated pure MMA droplet using reference spectra from the NIST database [21] and own reference spectra [23].

between 573 and 873 K. Before starting an experiment, the experimental setup is flushed with N_2 for at least 20 min to ensure an oxygen-free environment.

With a feeding system, fresh PMMA granules with a particle size of 1.5–2 mm are continuously supplied into the reactor. The gas-tight feeding system consists of a material storage, a screw conveyor, and a metering adapter, where the solid particles are mixed with an additional N_2 purge gas stream (20 l h^{-1}, standard conditions) to support the gravitational transport. By changing the rotation speed of the screw, the mass flow of PMMA particles can be controlled and is set to $\dot{m} = 3.33$ mg s^{-1} within this study. The mass flow is kept constant for the entire duration of the experiment ($\Delta t = 100$ min), resulting in a total mass $m_{PMMA} = 20$ g of PMMA particles fed into the reactor. The PMMA particles heat up to the bed temperatures with up to 10^3 K s^{-1}, react inside the fluidized bed, and stay there until final decomposition. Due to the lack of optical access, it is not possible to observe any structural changes of the particles (e.g., abrasion, fragmentation, or melting).

To estimate the particle heating rate, a transient differential equation for the particle temperature T_p is solved:

$$\underbrace{m_p \cdot c_p \cdot \frac{dT_p}{dt}}_{\text{heat-up}} = \underbrace{\alpha \cdot S_p \cdot (T_g - T_p)}_{\text{convection}} + \underbrace{\dot{Q}_{rad}}_{\text{radiation}} + \underbrace{\frac{dm_p}{dt} \cdot \Delta h_{reac}}_{\text{reaction}} \quad (4)$$

Within the energy balance, convective and radiative heat flows as well as a heat sink through the endothermic pyrolysis reaction are considered. Variables in Eq. (4) are the particle mass m_p, the specific heat capacity $c_p = 1470$ J kg^{-1} K^{-1}, the particle surface S_p (calculated for a spherical particle with diameter d_p), and the local surrounding gas temperature T_g. The endothermic reaction enthalpy Δh_{reac} sums the depolymerisation enthalpy $\Delta h_{depol} = 540$ kJ kg^{-1} [26] and the evaporation

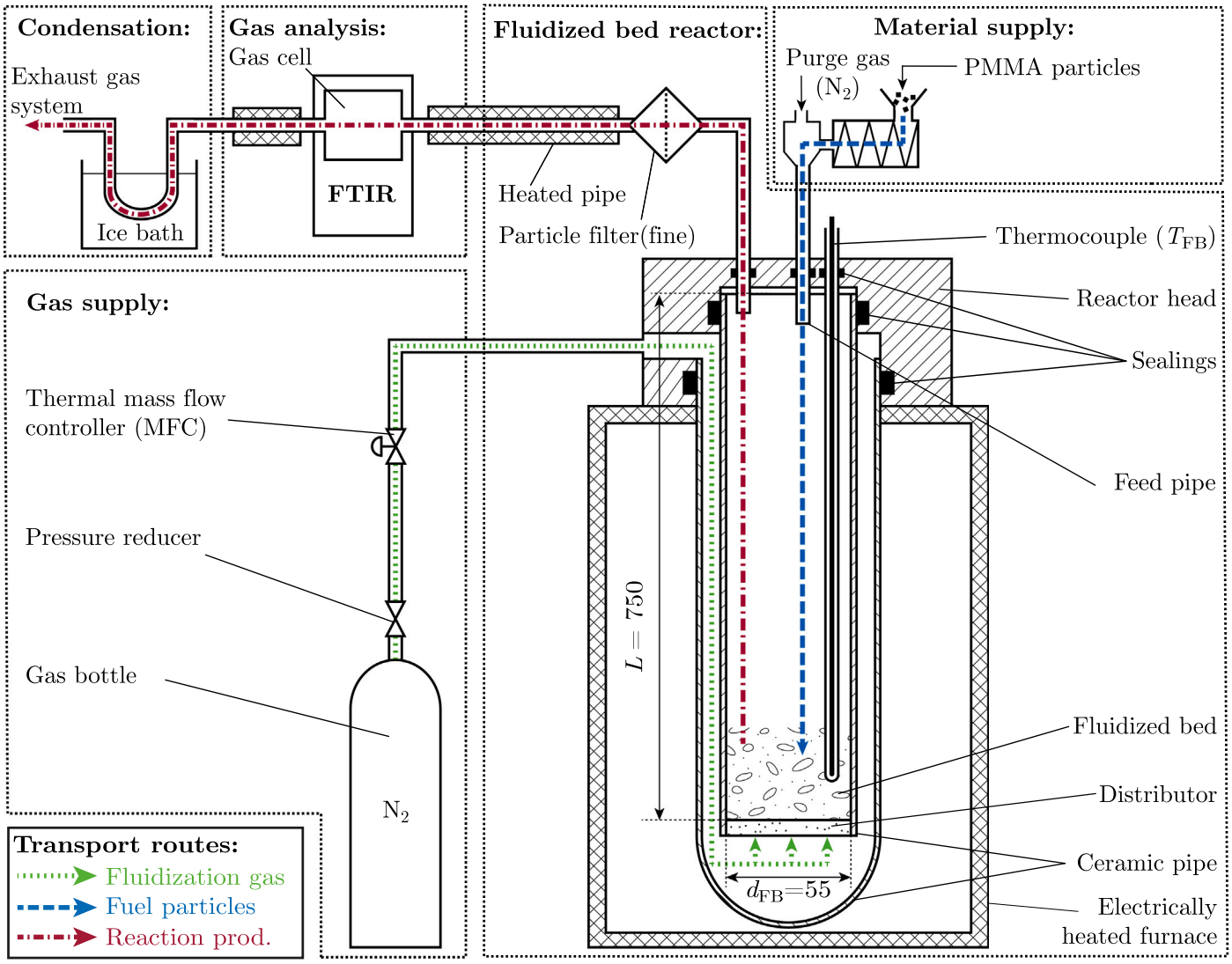

Fig. 6. Fluidized bed reactor setup for pyrolysis experiments (based on [19]).

enthalpy Δh_{evap} = 333 kJ kg^{-1} of MMA [27]. For the convective heat transfer α, the correlation from Gunn [28] is used in combination with the Ackermann correction [29] to account for the interaction during simultaneous heat and mass transfer. Detailed descriptions of the applied correlations for the heat transfer coefficient α and the radiative heat flow $\dot{Q}_{rad}$ are given in Pielsticker et al. [30].

The produced pyrolysis gases leave the reactor through a vertical tube in the reactor head, pass a particle filter, and are guided through heated pipes first to the Fourier-transform infrared spectrometer for gas analysis and second to an ice bath for separation of permanent light gases and condensable products. The heated pipes (453 K) before the FTIR and the ice bath minimize condensation of the reaction products before the desired condensation in the ice bath. The ice bath consists of four borosilicate glass U-tubes connected in series and surrounded by ice water. The exit temperature of the condensation unit is measured with a thermocouple and was found to be below 280 K in all experiments. The remaining light gases are sucked by an exhaust gas system. After the feeding time (100 min), the measurement is continued for 5 min to capture all reaction products in the FTIR and condensation unit. Within the current study, the influence of pyrolysis temperature on product yield and spectrum is investigated by changing the bed temperature from 573 to 873 K.

2.4. Evaluation

The quantitative determination of the PMMA pyrolysis products is performed similarly to the determination of the captured MMA yield in the validation procedure. Within the first step, volume fractions of relevant gas species, namely water (H_2O), carbon dioxide (CO_2), carbon monoxide (CO), methane (CH_4), ethane (C_2H_6), ethylene (C_2H_4), propane (C_3H_8), propylene (C_3H_6), butane (C_4H_{10}), formaldehyde (CH_2O), methanol (CH_3OH), ethanol (C_2H_5OH), and MMA ($C_5H_8O_2$) are calculated via regression analysis from the recorded IR spectra. Fig. 7 shows the obtained profile from one pyrolysis experiment at 723 K for the four most prominent species CO, CO_2, C_3H_6, and $C_5H_8O_2$. The experiment can be divided into a transient part in the beginning and a stationary phase starting at around 45 min. Within the stationary phase, strong periodic fluctuations are still visible, whereby the frequency can be traced back to the rotation of the screw conveyor. The transient behavior at the beginning is probably due to chemical and physical reasons. During thermal decomposition, various initiation, propagation, and termination reactions take place, which are controlled by reaction kinetics in the present temperature range [31]. Since at the beginning only pure polymer material is present in the reactor, but no decomposition products (e.g., oligomers), the observed decomposition products

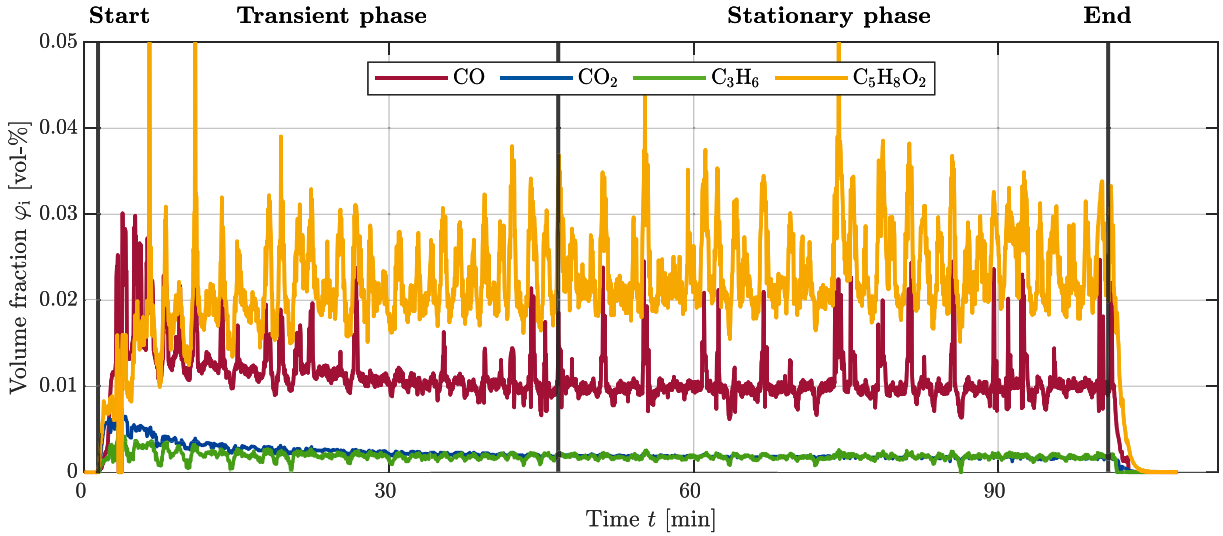

Fig. 7. Measured volume fractions of prominent pyrolysis products from PMMA pyrolysis at 723 K and an indication of different reaction phases separated by gray, vertical lines. (For interpretation of the references to colour in this figure legend, the reader is referred to the web version of this article.)

are initially dominated by small gas molecules (e.g., CO and CO_2) from the initiation reactions. With progressive decomposition, more and more MMA is formed as a product of the propagation reactions. However, the volume fraction represents the cumulative product spectrum from reactions with different reaction progress. As time progresses, the different stages of the reaction process are more and more evenly distributed in the reactor and ensure that a stationary behavior can be observed. However, it should be noted that this status does not represent the thermal equilibrium of the system.

The regression analysis is followed by a mass balance around the reactor system. Therefore, Eq. (2) is extended to account not only for MMA but also for the 12 other gas species. The mass-specific product yield y_i of the ith species (in $\mathrm{kg_i/kg_{PMMA}}$) is calculated with the mass flow $\dot{m}$, the experiment duration $\Delta t = t_{\mathrm{end}} - t_{\mathrm{start}}$, and the total N_2 volume flow $\dot{V}_{N_2} = 100\ \mathrm{l\ h^{-1}}$ (standard conditions) according to Eq. (5):

$$y_i = \frac{\rho_{N_2} \cdot M_i}{M_{N_2}} \cdot \frac{\dot{V}_{N_2}}{\dot{m}_{\mathrm{PMMA}} \cdot \Delta t} \cdot \int_{t_{\mathrm{start}}}^{t_{\mathrm{end}}} \frac{\varphi_i(t)}{\sum_{j=1}^{13} 1 - \varphi_j(t)}\, dt \tag{5}$$

Hereby, the implicit assumptions that

(a) fluidizing gas consists of pure nitrogen,
(b) temperature and pressure inside the cell are constant,
(c) all produced gases flow through the FTIR, and
(d) ideal gas law applies to all species

are made.

2.5. Condensate analysis method

For the captured liquid condensate, the mass is determined by weighing. Afterward, small samples of the condensate are further chemically analyzed with a mass spectrometer coupled to a gas chromatograph unit (GC–MS). For the gas chromatographic analysis, a *Trace 1310 GC* from *Thermo Fisher Scientific* equipped with an *Rtx-1 Pona* capillary column (length 50 m, inner diameter 0.25 mm, film thickness 0.5 µm) from *Restek* and a thermal conductivity detector is used. The column consists of dimethylpolysiloxane as the stationary phase while being flowed by helium as the mobile phase. The column is preheated to 323 K, then heated to 493 K with a heating rate of 8 K $\mathrm{min^{-1}}$ once the sample is injected and afterward hold at 493 K until the end of the measurement. Samples (1 ml) of the captured condensate are diluted 1:10 with acetone before being injected in the GC. Mass spectrograms are recorded for selected peaks in the GC signal. The analysis is undertaken with a *Thermo Scientific ISQ Single Quadrupole* mass spectrometer using 70 eV kinetic energy and a measurement time of 400 ms. This allows for the quantification of ionic fragments in the mass-to-charge ratio range 33–500 m/z. Based on the obtained data from MS, first, potential candidates of the condensate are determined. For selected components – methyl methacrylate (MMA), methyl acrylate (MA), methyl propionate (MP), methyl isobutyrate (MIB), and styrene – the GC setup is calibrated to allow a quantitative determination of the components.

3. Results and discussion

Based on the pyrolysis experiments with PMMA carried out at five different temperatures, first the reproducibility of the system and the evaluation routine are checked. Afterward, the influence of temperature on the product spectrum is determined in a quantitative manner and a comparison with available decomposition mechanisms is made. All experimental results are provided as open-access data [32].

3.1. Reproducibility of the reactor system

To analyze the reproducibility of the reactor system and possible fluctuations, three pyrolysis experiments under the same boundary conditions at $T_{\mathrm{FB}} = 723$ K are carried out. For all three experiments, the sum of all detected species is $y_{\mathrm{vol}} = 1.07 \pm 0.01$. The slight overprediction of the total volatile yield results mainly from the challenging determination of the correct CO volume fraction in the gas mixture as CO and MMA show strongly interfering absorption lines (cf. Fig. 3).

Fig. 8 shows the obtained pyrolysis yields of the different gas species. Out of the 13 analyzed species, 12 positive yields are calculated. The measured volume fraction profile of water vapor shows noise only and is thus discarded in the evaluation process to calculate the yields. With $y_{\mathrm{MMA}} = 0.78$, the monomer MMA has the highest yield across all products. The next dominant products are CO ($y = 0.108$), CO_2 ($y = 0.035$), C_3H_6 ($y = 0.027$), and CH_3OH ($y = 0.023$) with yields of at least 1 %. All other products show yields below 1 % at this temperature. However, at higher temperatures also CH_4 and CH_2O become important products with yields significantly above 1 %.

A comparison between the yields of the three runs reveals very similar results. This indicates, that the setup provides reproducible results. Further on, the results show that the fluctuations in the continuous

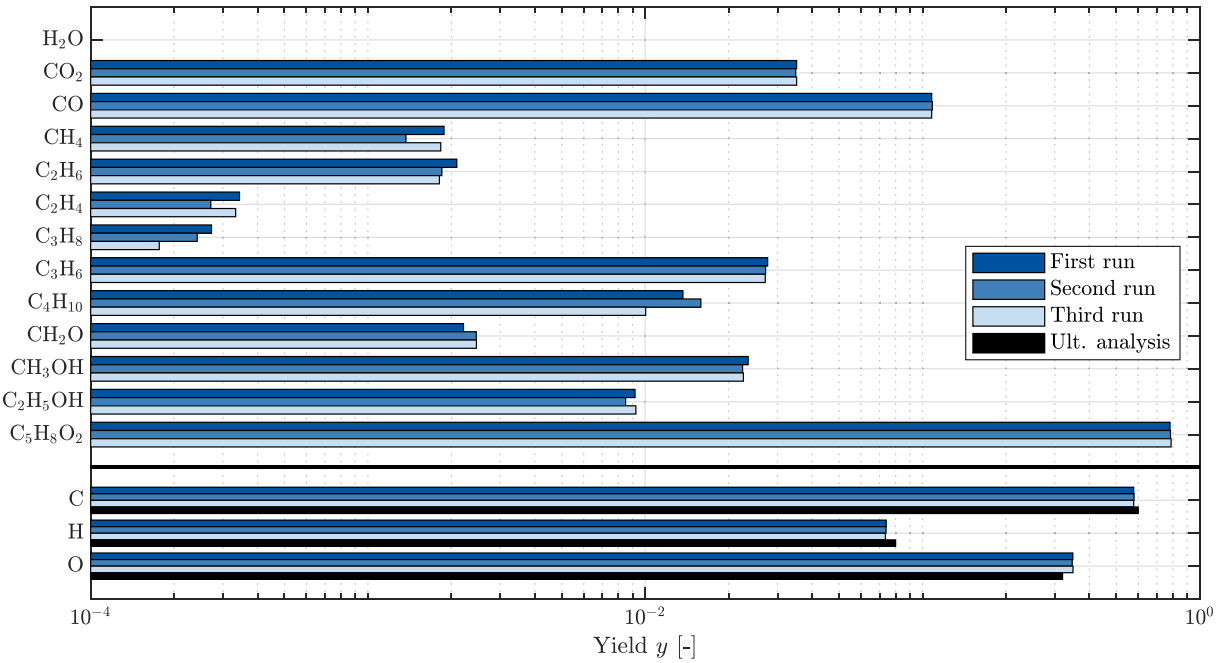

Fig. 8. Pyrolysis yields from three repetitive runs at a bed temperature of T_{FB} = 723 K in addition to determined elemental products in comparison with ultimate analysis results.

feeding system level out over time and have no impact on the overall observable yield. The knowledge of the single species yields and the corresponding molecular formula allows the calculation of the elemental yields divided into carbon, hydrogen, and oxygen. The comparison of the elemental yields shows even lower fluctuations between the three runs. This strengthens the plausibility of the results as different reactions taking place may slightly shift the single species results, but keep the overall number of atoms constant. The comparison with theoretical composition from ultimate analysis (mass fractions in kg/kg: C = 0.6, H = 0.08, O = 0.32) gives a slight overprediction of oxygen (y_O = 0.35) at the expense of carbon and hydrogen. This can result from uncertainties in the regression analysis to determine the gas composition, trace parts of oxygen in the fluidizing gas, or impurities in the raw material.

3.2. Temperature dependency of pyrolysis products

After having proven the reproducibility of the experimental setup and evaluation procedure, the influence of temperature on the product spectrum is investigated. Experiments at five different bed temperatures ranging from 573 to 873 K are undertaken. Fig. 9 shows the single

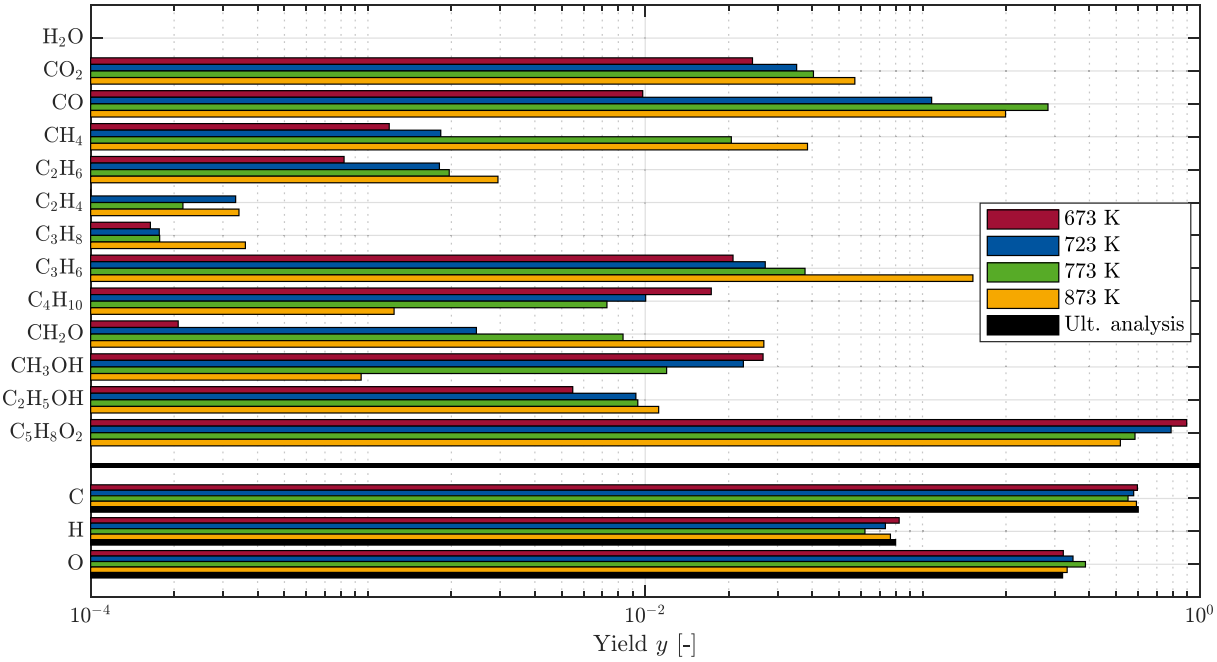

Fig. 9. Pyrolysis yields from runs at four different bed temperatures in addition to determined elemental products in comparison with ultimate analysis results.

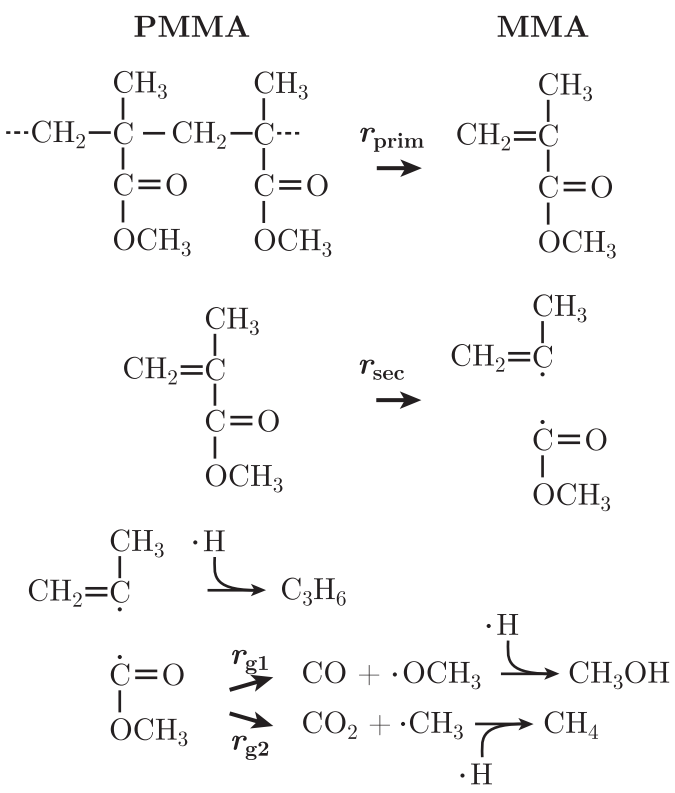

Fig. 10. Reaction scheme of PMMA and MMA decomposition based on Zeng et al. [33].

species and elemental yields as a function of bed temperature, but only for the experiments at 673, 723, 773, and 873 K. At a bed temperature of T_{FB} = 573 K, the experiment had to be aborted since no stationary phase was obtained until the end of the feeding time. Further on, the measured concentrations did not reach $\varphi_i = 0$ again within 10 h of operation. This reaction behavior indicates a very slow decomposition rate and requires further adoption of setup and operation routine to obtain a reliable product spectrum at this temperature.

The product yields at the remaining four temperatures reveal clear trends for all species except the CO yield at 773 K. As CO absorbs radiation in the wavenumber range from 1950 to 2300 cm^{-1}, strong interferences with the MMA absorption are unavoidable (see Fig. 3), but no alternative evaluation region is available. A higher pyrolysis temperature favors the decomposition of the monomer into fragments via secondary decomposition reactions. While reaching a monomer yield of approximately 90 % at 673 K, the MMA yield drops to 50 % at 873 K. In return, the yields of CO, CO_2, CH_4, and C_3H_6 increase. With regard to the total detected volatile content, a slight increase to up to $y_{vol} = 1.2$ can be observed for individual experiments at higher temperatures. This overestimation of the mass balance is due to the difficulty in determining the correct CO volume fraction in the presence of a high MMA fraction, as strong overlapping of the absorption lines can be observed here. An improvement in the overall mass balance can be achieved if all volume fractions are reduced (e.g., by reducing the PMMA mass flow). However, this has a counter-productive effect on the achievable amount of condensate, so that a slight overestimation of the mass balance is accepted here as a compromise.

The obtained product spectrum fits well with a proposed decomposition mechanism by Zeng et al. [33] for inert conditions (argon atmosphere), illustrated in Fig. 10.

Within the primary reaction step, the PMMA polymer is decomposed into its monomer building block MMA. With the ongoing decomposition of MMA via secondary gas-phase reactions, different radicals are formed that finally end up in the products CO and CO_2, as well as C_3H_6, CH_3OH, and CH_4 once hydrogen addition takes place. While considering hydrogen subtraction for the $\cdot OCH_3$ radical, also the formation of CH_2O is explainable, which is a significant product at higher temperatures in the experimental results.

3.3. Interaction of primary and secondary pyrolysis reactions

The experiments shown in Sections 3.1 and 3.2 are the result of primary PMMA decomposition and secondary gas-phase reactions. The following section analyzes the interaction of both phenomena at different temperatures and reaction times. Since chemical recycling of polymers is often designed for high recovery of the monomer, the MMA yield is of particular interest [9]. Fig. 11 shows the experimentally obtained MMA yield as a function of temperature in comparison with other experimental literature data as well as model predictions considering primary and secondary decomposition reactions.

The literature data and the experimental data of this study reveal two trends. For temperatures below 650 K, the study from Chub et al. [13] shows an increasing MMA yield with increasing temperature. For temperatures above 650 K, all other data points reveal a decrease in the obtained MMA yield with increasing temperature. Both trends can be well explained by using the first part of the reaction scheme from Fig. 10, where MMA is formed by PMMA pyrolysis (reaction rate r_{prim}) and then subsequently decomposed (reaction rate r_{sec}) into smaller fragments. The yield of MMA can be calculated by the differential equation

$$\frac{dy_{MMA}}{dt} = r_{prim} \cdot y_{PMMA} - r_{sec} \cdot y_{MMA} \tag{6}$$

in combination with an Arrhenius approach for the two reaction rates

$$r = A \cdot \exp\left(\frac{-E_a}{R \cdot T}\right), \tag{7}$$

wherein A is the pre-exponential factor, E_a the activation energy, R the universal gas constant and T the temperature. For the primary decomposition reaction, kinetic parameters from the study by Ferriol et al. [34] ($A = 1.67 \times 10^{14}$ s^{-1} and $E_a = 201$ kJ mol^{-1}) are used. Further, it assumed that no solid residual char is formed during PMMA pyrolysis [17] and all primary formed volatiles consist of MMA only. Since the present study is limited to the prediction of the MMA yield, the further decomposition reactions of the secondarily formed products (r_{g1} and r_{g2}) are not relevant, but would have to be considered in a detailed modeling of the entire product spectrum.

Fig. 11 includes the predicted MMA yields for the boundary conditions of the study by Chub et al. [13], where a residence time of the solid particles t_p = 10–45 min is given. The comparison of model prediction and experimental data shows that the process under these conditions is limited by the primary decomposition rate. The reported significant amounts of unreacted PMMA support our conclusion that the used residence times of 10–45 min are too short to reach full decomposition.

The model predictions can further explain the observed experimental results in this study: The vertical dotted line at T = 573 K crosses the two model predictions with t_p = 100 min and t_p = 10 h at yields of $y_{MMA} \approx 0.4$ and $y_{MMA} \approx 0.95$, respectively. The two times reflect the total feeding time and the overall experimental duration until the termination. The model predictions confirm the experimental observations that even after t_p = 10 h no complete conversion has been achieved and new decomposition products can still be detected. However, for temperatures above 650 K, a reaction time of 5 min is sufficient to observe the full conversion of PMMA into its pyrolysis products. This hypothesis is supported by the well-closed elemental mass balance in Figs. 8 and 9. Based on this, the observed experimental MMA yields for the temperature range $T \geq 673$ K cannot be limited by the primary pyrolysis process.

To evaluate the role of secondary gas-phase reactions, the decomposition of MMA into smaller fragments (see Fig. 10) is calculated assuming

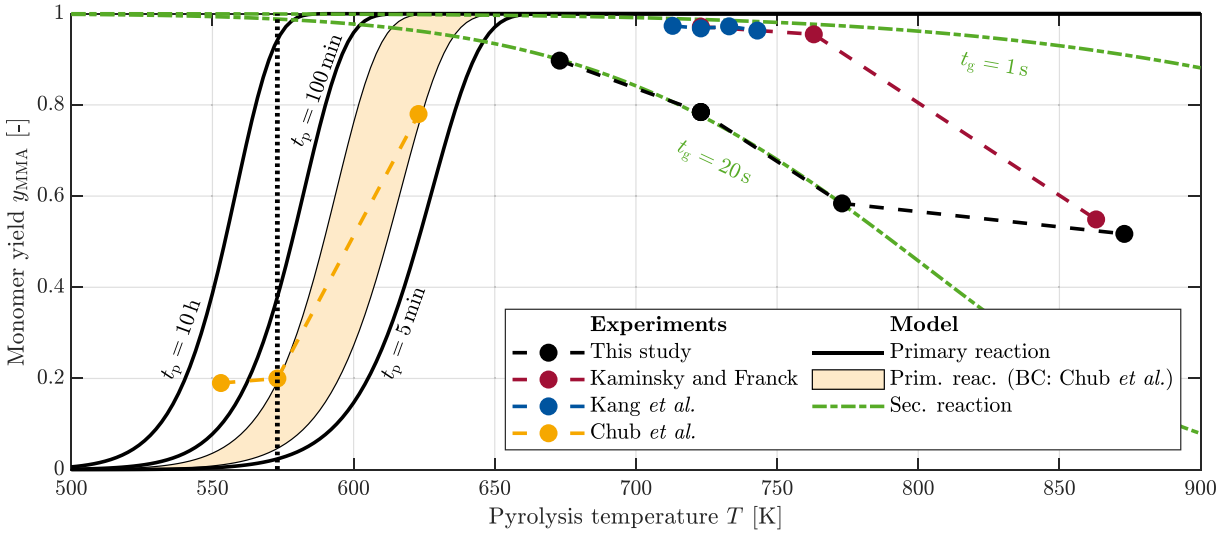

Fig. 11. Experimental MMA yields from PMMA pyrolysis (this study and literature: Kaminsky and Franck [10], Kang et al. [11], and Chub et al. [13]) as a function of temperature in comparison with model predictions for primary PMMA pyrolysis and secondary MMA gas-phase decomposition. Kinetic parameters for primary reaction are taken from Ferriol et al. [34], while the secondary decomposition kinetics are fitted to the experimental results. The orange area represents simulation results for the boundary conditions of Chub et al. [13]. (For interpretation of the references to colour in this figure legend, the reader is referred to the web version of this article.)

a first-order decomposition mechanism according to Eq. (6). In contrast to the decomposition of PMMA, reaction kinetic parameters of MMA are not available in the literature to the best of the authors' knowledge. The experimental data measured by Forman et al. [35] can be used to calculate a rate $r_{sec} \approx 7.5 \times 10^{-3}$ s^{-1} at 773 K. Thus, kinetic parameters for the secondary pyrolysis reaction are estimated based on experimental data from this study and other literature data [10,11]. The secondary decomposition strongly depends on the gas residence time t_g under hot conditions. For the present study, the gas residence time is in the range t_g = 20–30 s. The other two studies from Kaminsky and Franck [10] and Kang et al. [11] report gas residence times in the range t_g = 0.5–1 s. Fig. 11 shows that kinetic parameters $A_{sec} = 1.53 \times 10^3$ s^{-1} and $E_{a,sec}$ = 70.4 kJ mol^{-1} explain the MMA yields for all experimental points at temperatures $T \leq 773$ K. However, at $T \approx 870$ K the model strongly overpredicts the decomposition for the data of Kaminsky and Franck [10] and at the same time strongly underpredicts the decomposition in the present study. Potentially, the simplified assumptions of already fully decomposed PMMA as well as a fixed residence time under a constant reaction temperature do not reflect the real experimental boundary conditions correctly, where, e.g., the gas residence time follows a distribution and reactor temperature is locally dependent.

Also, the assumption that the primary pyrolysis step is fully controlled by the reaction kinetics might be questionable as transport phenomena such as heat transfer to the particle surface and inside the particle may limit the available enthalpy for the reaction [12,36].

3.4. Interaction of heat transfer and reaction kinetic limitations

Whether the conversion process is controlled by intrinsic reaction kinetics or heat transfer (internal and/or external), can be estimated with the dimensionless pyrolysis numbers Py_I and Py_{II} defined in Eqs. (8), (9) [37,38]. They express the ratio of time scales between heat transport and reaction process.

$$Py_I = \frac{4 \cdot \lambda_p}{\rho_p \cdot c_p \cdot d_p^2 \cdot r} \tag{8}$$

$$Py_{II} = \frac{2 \cdot \alpha}{\rho_p \cdot c_p \cdot d_p \cdot r} \tag{9}$$

Material properties of the solid PMMA particles such as the thermal conductivity λ_p = 0.2 W m^{-1} K^{-1}, density ρ_p = 1180 kg m^{-3}, and specific heat capacity c_p = 1470 J kg^{-1} K^{-1} are assumed. Particle diameter d_p = 2 mm is taken conservatively. To determine the convective heat transfer coefficient α, the correlation from Gunn [28] is used, which was developed for single particles immersed in a fluidized bed. Within the study from Gövert [39] different correlations have been tested and the one mentioned above was identified to show the best performance for the present setup. The reaction rate r is calculated based on the Arrhenius approach from Eq. (7) using the kinetic parameter set from Ferriol et al. [34].

Fig. 12 shows the two dimensionless Py numbers as a function of temperature. Within the investigated temperature range, the externally controlled Py_{II} number is always smaller than the internally controlled Py_I number, indicating that the convective heat transfer acts as the dominating limitation factor for the heat transfer, meaning that the Biot number is smaller than one. Further on, Fig. 12 reveals that the pyrolysis is controlled by the heat transfer for temperatures above $T > 730$ K indicated with $Py < 0.1$. Within the present study, only the experiment at 573 K is strongly controlled by the reaction kinetics ($Py > 10$). The temperatures in between lie in the transition zone indicated by similar time scales of heat transfer and reaction process.

Fig. 13 illustrates simulation results from the particle model based on the energy balance given in Eq. (4). The relative time t^* sets conversion and heat-up times of the limited cases with coupled mass and energy balances in relation to the 95 % conversion time of the unlimited reaction process assuming a constant isothermal particle temperature equal to that of the fluidized bed. For conversion, the corresponding time is calculated once 95 % mass release is reached and for the heat-up once the particle temperature approaches 95 % of the bed temperature. Both indicators are given for two particle sizes (d_p = 1 and 2 mm) and support the observations from Fig. 12. Only for the reactor temperature T = 573 K, the reaction process is purely controlled by the reaction kinetics, indicated by identical reaction times for the limited and unlimited case. In this case, the heat-up process is orders of magnitude faster than the reaction. For the two highest temperatures (and both particle sizes), the heat-up lasts throughout the entire conversion process indicated by $t^* \approx 1$. In these cases, the particle reaches an equilibrium, where endothermic reaction and the heat transfer to the

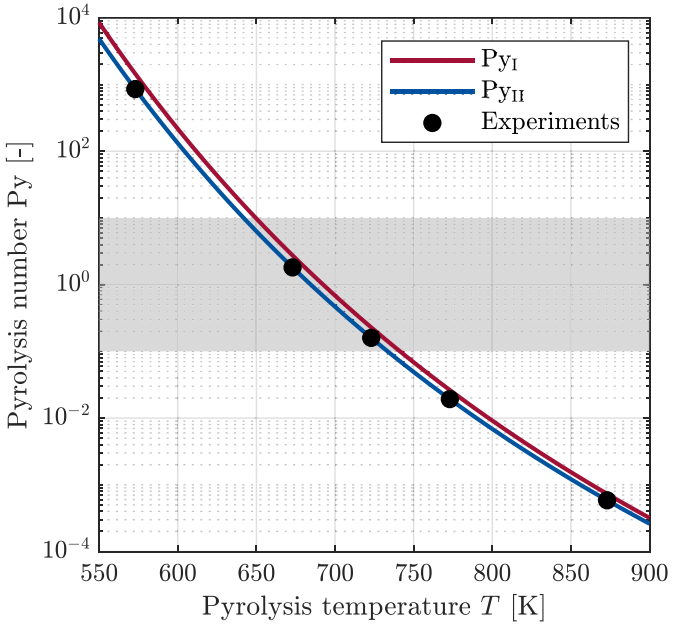

Fig. 12. Dimensionless pyrolysis numbers characterizing limitations by heat transfer and reaction kinetics.

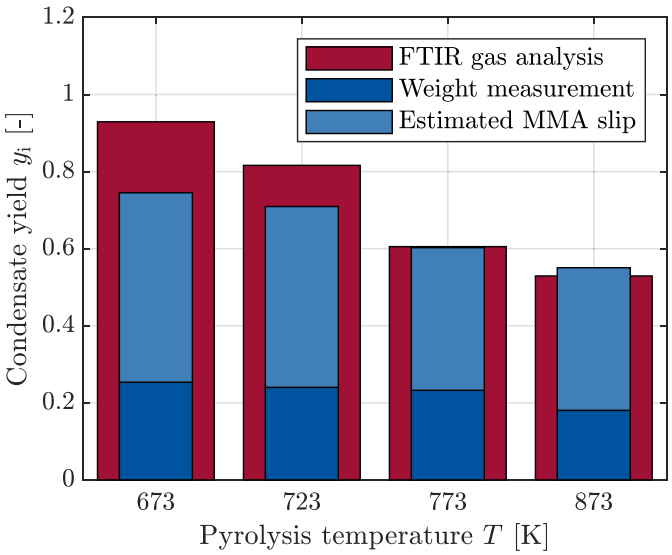

Fig. 14. Expected condensate yields calculated based on the FTIR gas analysis in comparison with weighted condensate and estimated slip.

particle compensate each other. This enlarges the conversion times to multiple orders of the conversion time under ideal conditions. For the reactor temperature $T = 673$ K, the heat-up times are significantly shorter than the reaction times but still have a small influence on the observed conversion.

As the current particle model assumes a homogeneous particle temperature, effects of particle-internal heat transfer limitations cannot be captured. Furthermore, the simulations do not consider any changes in, e.g., particle size, shape, or aggregate state and thus only give a simplified representation of the process. For real applications, phase transition effects such as melting and film formation or inclusion of gas bubbles may play a significant role in the limitations. Unfortunately, the given data in the mentioned literature studies do not allow for a detailed analysis of limitations. However, the used particle sizes (d_p = 1–1.5 mm [11] and d_p = 0.5–1.5 mm [10]) reveal that the process is also limited by heat transfer.

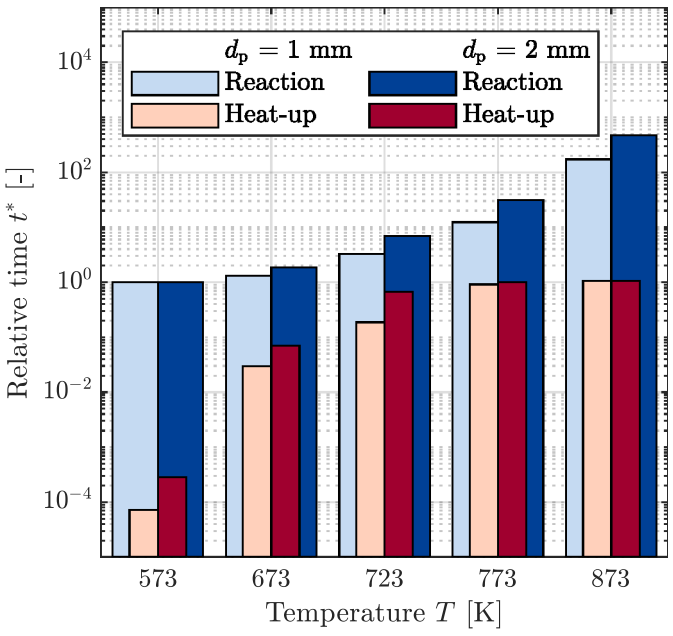

Fig. 13. Relative times for 95 % conversion and heat-up in relation to the conversion time under ideal conditions for two particle sizes at different reactor temperatures.

3.5. Condensate analysis

With the condensation unit described in Section 2.3, condensable reaction products of the PMMA pyrolysis process can be captured for further detailed analysis. Fig. 14 shows the comparison of captured yields in the condensation unit compared to the yields from the FTIR gas analysis previously described.

The condensate yield based on the FTIR gas measurements is calculated by summing up the yields for species with condensation temperatures above 273 K (ice bath temperature) including MMA, ethanol, and methanol. Obviously, the weighted condensate yields are significantly lower than the yields determined by the FTIR gas analysis. However, due to the constructional limitations of the gas condensation unit, some gas components stay in the gaseous phase and thus escape through the outlet of the cooler. By assuming that the outlet volume fraction is equal to saturation conditions for the cooler outlet temperature, the yields not detected by the weight measured are estimated. As can be seen, these undetected yields are higher than the weight measurements and can well close the gap to the FTIR-based yields at higher temperatures. For lower temperatures, mass differences up to 18 % are visible. A potential reason might be the slightly fluctuating outlet temperature of the cooler in the ice bath, which can be improved by using an intensive cooling unit with a lower temperature. However, optimization of the condensation unit is not the main focus of this study.

The captured condensate samples are subject to a subsequent analysis via GC–MS as described in Section 2.5. Fig. 15 shows the quantitatively obtained composition of the samples taken for different pyrolysis temperatures. The main component in all samples is MMA ranging from 88 % to 95 %. The other four calibrated species sum up to approximately 1.9 %–3.5 % with MA being the most prominent. The domination of MA in the minor liquid products was already observed in the studies by Kaminsky and Franck [10] and Kang et al. [11] and attributed to the usage of MA as a copolymer in the production process. In both studies and the present one, a slight increase with increasing temperature is visible.

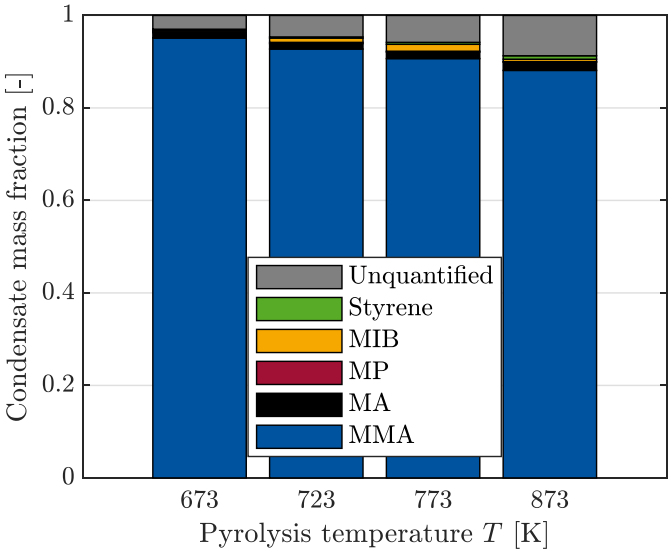

Fig. 15. Quantitative analysis based on GC-MS of the condensate captured at different pyrolysis temperatures.

With increasing pyrolysis temperature, more of the overall side products are formed and the amount of unquantified species increases, while no clear trend for the other quantified species can be derived.

4. Conclusion

Within the present study, an existing small-scale fluidized bed reactor coupled with FTIR gas analysis was successfully adapted for the quantitative determination of pyrolysis products from polymethyl methacrylate. To measure reliable concentrations of the main reaction product methyl methacrylate (MMA) in the off-gas stream of the reactor, the FTIR spectrometer was first calibrated with an MMA/N_2 gas mixture of various concentrations, which was generated by cooling a loaded gas stream to a well-known saturation temperature. Afterward, the newly recorded spectra were included in the evaluation procedure and were cross-checked with pure MMA samples of known mass evaporated in a heated line before the FTIR. A significant improvement in correctly closing the mass balance could be achieved with the new reference spectra compared to the initially available reference spectra from the NIST database.

After improving the FTIR measurement technique for the quantitative MMA detection, pyrolysis experiments of fresh PMMA granules with a continuous fuel feed were performed at reactor temperatures between 573 and 873 K. The reproducibility of the system and the reliability of the results have been proven by three independent repetitions and a comparison of the overall elemental yields. The correct quantitative determination of the products can be verified by the well-closed mass balance for a gas-phase-based analysis of pyrolysis reactions, reaching values between y_{vol} = 0.97–1.2. The slight overestimation, especially for higher temperatures, results from the strong interference of CO and MMA absorption lines, making the correct determination of volume fractions challenging. Mass-specific yields of 13 reaction products could be determined, with MMA, CO, CO_2, CH_4, C_3H_6, CH_3OH, and CH_2O being the most dominant species. All of these species fit well into already proposed decomposition mechanisms of MMA into smaller fragments. An increase in temperature has shown a shift from approximately 90 % MMA yield down to 50 %, which was accompanied by an increase in the before-mentioned light gas decomposition products. The comparison with available literature data revealed lower MMA yields in the higher temperature range in this study, which was explained by an increased hot gas residence time. A decomposition kinetic for MMA into smaller molecules has been derived. In contrast, a limitation of the MMA yield was identified for temperatures below 650 K due to the reaction kinetics of the primary PMMA decomposition by available literature data for kinetic reaction parameters. Using a coupled energy and mass balance of a particle model, it was also possible to show that the pyrolysis process for the PMMA particles investigated takes place in regime limited by heat transfer. Parts of the liquid product fraction have been captured for subsequent GC–MS analysis. The analysis confirmed the high purity of the captured condensate allowing feedback into the polymerization process.

The results have highlighted two important aspects influencing the final product spectrum of PMMA pyrolysis: the primary decomposition rate of the PMMA polymer and the secondary gas-phase reactions of the formed MMA molecules. The quantitative online gas analysis via FTIR spectroscopy allows to gain further insights into both aspects. If continuous dosing is replaced by batch experiments, the time-dependent evolution of the gas species allows conclusions to be drawn about the present decomposition rate of the polymer, which has already been intensively used in biomass pyrolysis [18,19]. By using pure MMA samples as feed and varying the residence time, gas-phase reaction kinetics can be determined to extend existing decomposition mechanisms and verify the proposed kinetic parameter set.

CRediT authorship contribution statement

Stefan Pielsticker: Writing – original draft, investigation, conceptualization. **Katja Hendricks:** Visualization, investigation. **Christoph Knevels:** Investigation. **Marcus S. Lehnertz:** Writing – review & editing, methodology. **Regina Palkovits:** Writing – review & editing, supervision, funding acquisition. **Reinhold Kneer:** Writing – review & editing, supervision, funding acquisition.

Declaration of competing interest

The authors declare that they have no known competing financial interests or personal relationships that could have appeared to influence the work reported in this paper.

Acknowledgments

The authors thank the Exploratory Research Space – ERS, RWTH Aachen for funding under grant agreement (PFKA008) “Cluster 4 Plastics Recycling“. S.P. and R.K. acknowledge funding by the German Research Foundation (DFG) – project number (215035359) – within the CRC/TRR 129 “Oxyflame”. M.L. and R.P. acknowledge funding by Werner Siemens Foundation in the frame of the WSS research center “catalaix: catalysis for a circular economy.”

Data availability

Data is available under https://doi.org/10.18154/RWTH-2024-08099.

References

[1] Merchan AL, Fischöder T, Hee J, Lehnertz MS, Osterthun O, Pielsticker S, et al. Chemical recycling of bioplastics: technical opportunities to preserve chemical functionality as path towards a circular economy. Green Chem 2022;24:9428–49. doi:https://doi.org/10.1039/D2GC02244C.
[2] Biessey P, Vogel J, Seitz M, Quicker P. Plastic waste utilization via chemical recycling: approaches, limitations, and the challenges ahead. Chem Ing Tech 2023;95:1199–214. doi:https://doi.org/10.1002/cite.202300042.
[3] Darko C, Yung PWS, Chen A, Acquaye A. Review and recommendations for sustainable pathways of recycling commodity plastic waste across different economic regions. Resour Environ Sustain 2023;14:100134. doi:https://doi.org/10.1016/j.resenv.2023.100134.
[4] Moens EKC, de Smit K, Marien YW, Trigilio AD, van Steenberge PHM, van Geem KM, et al. Progress in reaction mechanisms and reactor technologies for thermochemical recycling of poly(methyl methacrylate). Polymers 2020;12. doi:https://doi.org/10.3390/polym12081667.
[5] Achilias DS. Chemical recycling of poly(methyl methacrylate) by pyrolysis. Potential use of the liquid fraction as a raw material for the reproduction of the polymer. Eur Polym J 2007;43:2564–75. doi:https://doi.org/10.1016/j.eurpolymj.2007.02.044.

[6] Gkaliou K, Benedini L, Sárossy Z, Dalsgaard Jensen C, Henriksen UB, Daugaard AE. Recycled PMMA prepared directly from crude MMA obtained from thermal depolymerization of mixed PMMA waste. Waste Manage (Oxford) 2023;164:191–9. doi:https://doi.org/10.1016/j.wasman.2023.04.007.
[7] Ali U, Karim KJBA, Buang NA. A review of the properties and applications of poly (methyl methacrylate) (PMMA). Polym Rev 2015;55:678–705. doi:https://doi.org/10.1080/15583724.2015.1031377.
[8] de Tommaso J, Dubois J-L. Risk analysis on PMMA recycling economics. Polymers 2021;13. doi:https://doi.org/10.3390/polym13162724.
[9] Kikuchi Y, Hirao M, Ookubo T, Sasaki A. Design of recycling system for poly(methyl methacrylate) (PMMA). Part 1: recycling scenario analysis. Int J Life Cycle Assess 2014;19:120–9. doi:https://doi.org/10.1007/s11367-013-0624-y.
[10] Kaminsky W, Franck J. Monomer recovery by pyrolysis of poly(methyl methacrylate) (PMMA). J Anal Appl Pyrolysis 1991;19:311–8. doi:https://doi.org/10.1016/0165-2370(91)80052-A.
[11] Kang B-S, Kim SG, Kim J-S. Thermal degradation of poly(methyl methacrylate) polymers: kinetics and recovery of monomers using a fluidized bed reactor. J Anal Appl Pyrolysis 2008;81:7–13. doi:https://doi.org/10.1016/j.jaap.2007.07.001.
[12] Smolders K, Baeyens J. Thermal degradation of PMMA in fluidised beds. Waste Manage (Oxford) 2004;24:849–57. doi:https://doi.org/10.1016/j.wasman.2004.06.002.
[13] Chub OV, Saadatkhah N, Dubois J-L, Patience GS. Fluidized bed poly(methyl methacrylate) thermolysis to methyl methacrylate followed by catalytic hydrolysis to methacrylic acid. Appl Cat A Gen 2022;638:118637. doi:https://doi.org/10.1016/j.apcata.2022.118637.
[14] Sanders IC, Kuenning NM, Minesi NQ, Pineda DI, Spearrin RM. Methyl methacrylate thermal decomposition: modeling and laser spectroscopy of species time-histories behind reflected shock waves. Fuel 2023;335:126846. doi:https://doi.org/10.1016/j.fuel.2022.126846.
[15] Kaminsky W, Eger C. Pyrolysis of filled PMMA for monomer recovery. J Anal Appl Pyrolysis 2001(58–59:781–7. doi:https://doi.org/10.1016/S0165-2370(00)00171-6.
[16] Kashiwagi T, Inaba A, Brown JE, Hatada K, Kitayama T, Masuda E. Effects of weak linkages on the thermal and oxidative degradation of poly(methyl methacrylates). Macromolecules 1986;19:2160–8. doi:https://doi.org/10.1021/ma00162a010.
[17] Chen R, Xu M. Kinetic and volatile products study of micron-sized PMMA waste pyrolysis using thermogravimetry and Fourier transform infrared analysis. Waste Manage (Oxford) 2020;113:51–61. doi:https://doi.org/10.1016/j.wasman.2020.05.039.
[18] Pielsticker S, Schlögel KU, Kreitzberg T, Hatzfeld O, Kneer R. Biomass pyrolysis kinetics in a fluidized bed reactor: measurements and plausibility verification for reaction conditions. Fuel 2019;254:115589. doi:https://doi.org/10.1016/j.fuel.2019.05.172.
[19] Pielsticker S, Gövert B, Umeki K, Kneer R. Flash pyrolysis kinetics of extracted lignocellulosic biomass components. Front Energy Res 2021;9. doi:https://doi.org/10.3389/fenrg.2021.737011.
[20] Kreitzberg T, Pielsticker S, Hatzfeld O, Kneer R. Reactivity of biochar gasification in atmospheres of steam, carbon dioxide and their mixtures. In: Joint Meeting the German and Italian Sections of the Combustion Institute; 2018.
[21] NIST Chemistry WebBook: methyl methacrylate; 2023. https://webbook.nist.gov/cgi/cbook.cgi?ID=++80-62-6.
[22] Brockhaus VA, Jenckel E. Über die Kinetik des thermischen Abbaues von Polymethacrylsäuremethylester. Makromolekulare Chemie 1956;18:262–93. doi:https://doi.org/10.1002/macp.1956.020180124.
[23] Pielsticker S, Hendricks K, Kneer R. Fourier-transform infrared (FTIR) spectra of gaseous methyl methacrylate (MMA); 2024. doi:https://doi.org/10.18154/RWTH-2024-08098.
[24] Sugumaran D, Abd Karim KJ. Removal of copper (II) ion using chitosan-graft-poly(methyl methacrylate) as Adsorbent; 2017. doi:https://doi.org/10.13140/RG.2.2.33911.93601.
[25] Abrahamsen AR, Geldart D. Behaviour of gas-fluidized beds of fine powders: part I. Homog Expans Powder Technol 1980;26:35–46. doi:https://doi.org/10.1016/0032-5910(80)85005-4.
[26] Roberts DE. Heats of polymerization. A summary of published values and their relation to structure. J Res Natl Bur Stand 1950;221–32.
[27] Steele WV, Chirico RD, Cowell AB, Knipmeyer SE, Nguyen A. Thermodynamic properties and ideal-gas enthalpies of formation for trans-methyl cinnamate, α-methyl cinnamaldehyde, methyl methacrylate, 1-nonyne, trimethylacetic acid, trimethylacetic anhydride, and ethyl trimethyl acetate. J Chem Eng Data 2002;47:700–14. doi:https://doi.org/10.1021/je010086r.
[28] Gunn DJ. Transfer of heat or mass to particles in fixed and fluidised beds. Int J Heat Mass Transfer 1978;21:467–76. doi:https://doi.org/10.1016/0017-9310(78)90080-7.
[29] Ackermann G. Wärmeübergang und molekulare Stoffübertragung im gleichen Feld bei großen temperatur- und partialdruckdifferenzen, VDI-Forschungsheft. 1937;8:1–16.
[30] Pielsticker S, Ontyd C, Kreitzberg T, Hatzfeld O, Schiemann M, Scherer V, et al. Adaptation of the chemical percolation devolatilization model for low temperature pyrolysis in a fluidized bed reactor. Combust Sci Technol 2019;52:1–18. doi:https://doi.org/10.1080/00102202.2019.1682433.
[31] Barlow A, Lehrle RS, Robb JC, Sunderland D. Polymethylmethacrylate degradation – kinetics and mechanisms in the temperature range 340° to 460°C. Polymer 1967;8:537–45. doi:https://doi.org/10.1016/0032-3861(67)90065-1.
[32] Pielsticker S, Hendricks K, Knevels C, Lehnertz MS, Palkovits R, Kneer R. Experimental determination of quantitative yields from polymethyl methacrylate (PMMA) flash pyrolysis in a fluidized bed reactor via online FTIR gas analysis – supplementary dataset; 2025. doi:https://doi.org/10.18154/RWTH-2024-08099.
[33] Zeng WR, Li SF, Chow WK. Preliminary studies on burning behavior of polymethylmethacrylate (PMMA). J Fire Sci 2002;20:297–317. doi:https://doi.org/10.1177/073490402762574749.
[34] Ferriol M, Gentilhomme A, Cochez M, Oget N, Mieloszynski JL. Thermal degradation of poly(methyl methacrylate) (PMMA): modelling of DTG and TG curves. Polym Degrad Stab 2003;79:271–81. doi:https://doi.org/10.1016/S0141-3910(02)00291-4.
[35] Forman RL, Mackinnon HM, Ritchie PD. Studies in pyrolysis. Part XXV. Acrylic, methacrylic, and crotonic acid, and some derivatives: novel decarbonylation of αβ-unsaturated carboxylic acids. J Chem Soc C 1968;2013–6. doi:https://doi.org/10.1039/J39680002013.
[36] Sasse F, Emig G. Chemical recycling of polymer materials. Chem Eng Technol 1998;21:777–89. doi:https://doi.org/10.1002/(SICI)1521-4125(199810)21:10\TU\textless777::AID-CEAT777\TU\textgreater3.0.CO;2-L.
[37] Pyle DL, Zaror CA. Heat transfer and kinetics in the low temperature pyrolysis of solids. Chem Eng Sci 1984;39:147–58. doi:https://doi.org/10.1016/0009-2509(84)80140-2.
[38] Paulsen AD, Mettler MS, Dauenhauer PJ. The role of sample dimension and temperature in cellulose pyrolysis. Energy Fuels 2013;27:2126–34. doi:https://doi.org/10.1021/ef302117j.
[39] Gövert B. Char combustion kinetics using a micro fluidized bed reactor [Dissertation]. Aachen: RWTH Aachen University; 2018. doi:https://doi.org/10.18154/RWTH-2019-00500.